

Systematic Biases in Galaxy Luminosity Functions

Julianne J. Dalcanton^{1,2}

Observatories of the Carnegie Institution of Washington, 813 Santa Barbara Street, Pasadena CA, 91101

Accepted to the Astrophysical Journal

ABSTRACT

Both the detection of galaxies and the derivation of the luminosity function depend upon isophotal magnitudes, implicitly in the first case, and explicitly in the latter. However, unlike perfect point sources, the fraction of a galaxy's light contained within the limiting isophote is a function of redshift, due to the combined effects of the point spread function and cosmological dimming. This redshift variation in the measured isophotal luminosity can strongly affect the derived luminosity function. Using simulations which include the effects of seeing upon both disk and elliptical galaxies, we explore the size of the systematic biases which can result from ignoring the redshift variation in the fraction of detected light. We show that the biases lead to underestimates in the normalization of the luminosity function, as well as changes in shape. The size of the bias depends upon redshift, and thus can mimic galaxy evolution. Surprisingly, these biases can be extremely large *without* affecting $\langle V/V_{max} \rangle$. However, these biases can be detected in the full distribution of V/V_{max} , and in fact may have already been detected in recent surveys. Because the systematic biases result from the redshift variation in the fraction of lost light, the biases are not significant when the fraction of lost light is always small over the entire survey volume, for all galaxy types. However, as modern galaxy surveys now reach higher redshifts, lower surface brightnesses, and smaller angular sizes, the effects of seeing and galaxy visibility are becoming increasingly important and need to be taken into account. We show that the expected biases are not necessarily eliminated when using aperture magnitudes, FOCAS "total" magnitudes, or Kron magnitudes, but may be reduced significantly if Petrosian magnitudes are used. These considerations may also apply to samples of clusters selected in X-rays.

1. Introduction

The luminosity function remains one of the principal tools for quantifying the population of galaxies. The evolution of the luminosity function with redshift provides a critical test for assessing changes in the galaxy population with time. Variations in the galaxy luminosity function with environment, emission line strength, and morphological type all provide broad clues towards distinguishing among galaxy formation scenarios. Given that the usefulness of the luminosity function as a cosmological tool depends upon comparing luminosity functions at different times or for different galaxy types, it is extremely important that the measurement of the luminosity function be unbiased with redshift, galaxy morphology, or survey technique.

¹e-mail address: jd@ociw.edu

²Hubble Fellow

Standard approaches for calculating the luminosity function involve mathematical variants of what Binggeli et al. (1988) refer to as the “classical method”, wherein each galaxy is weighted by the inverse of the maximum volume over which it could have been detected, given the galaxy’s luminosity and the magnitude limit of the survey. Other methods which reduce the impact of spatial inhomogeneity on the derived luminosity function, such as Sandage et al.’s (1979) parametric maximum-likelihood method, calculate a likelihood based upon comparing the observed luminosity of each galaxy in the sample to the range of potentially observable luminosities at each galaxy’s redshift.

Both of these methods require estimating the range of absolute magnitudes which can be seen at each redshift, given the selection criteria of a survey. Any systematic error in this procedure can lead to a systematic mismeasurement of the luminosity function. As we will show here, typical procedures for measuring the luminosity function do indeed suffer from these systematic biases, largely due to a simplistic estimate of how a galaxy’s apparent magnitude varies with redshift.

Most determinations of the luminosity function assume that an isophotal magnitude is a good representation of the galaxy’s total magnitude, and that the isophotal magnitude varies with redshift as the inverse square of the luminosity distance (modulo k -corrections). While these are perhaps reasonable approximations for point sources in deep data with exceptional seeing, or for nearby surveys of extremely bright, high surface brightness galaxies, these assumptions break down for real galaxies in many modern surveys (e.g. McGaugh 1994). Some of a galaxy’s light is lost beyond the outer isophote of a galaxy image, due to the combined effects of seeing and surface brightness variations (both cosmological and intrinsic), leading to the apparent isophotal magnitude falling off more rapidly with redshift than predicted. Thus, field galaxy surveys can easily overestimate the effective volume of the survey, and therefore systematically underestimate the luminosity function. More importantly, the degree to which the derived luminosity function is underestimated is a strong function of galaxy size and surface brightness, as well as being redshift dependent. This can lead to apparent redshift evolution in the galaxy population, and to erroneous conclusions about the variation of the morphological mix within the galaxy population. The measured luminosity function can also depend upon seeing such that similar surveys with different imaging data (e.g. ground based vs. HST) can produce different results. While these biases can be mitigated against by using exceptionally deep imaging data or large aperture magnitudes, the majority of deep field surveys have used isophotal magnitudes to derive the luminosity function. Instead of isophotal magnitudes, some fraction of surveys have used corrected “total” magnitudes which choose an aperture size dynamically, based upon either the isophotal area or the intensity-weighted first moment radius. However, in the former case, the corrected “total” magnitude actually reduces to using an isophotal magnitude with a fainter limiting magnitude, as we will show in 6. Furthermore, even when isophotal magnitudes are not used for photometry, the selection of galaxies for a survey depends implicitly on the isophotal magnitude limit of the survey images, subjecting the derived luminosity function to many of the biases we explore here.

The importance of correcting for light lost beyond the limiting isophote has been long known (Humason et al. 1956), and has traditionally been studied through curve-of-growth analyses. Sandage (1961) explicitly warns against the use of isophotal magnitudes in cosmological tests, pointing out that they are not a consistent measure of galaxy flux at all redshifts. Until the recent era of deep redshift surveys, it has been sufficient to use growth curves to correct isophotal magnitudes onto the same magnitude system; since surveys covered only a limited range in redshift, once galaxy magnitudes were corrected to the same isophotal limit, a constant fraction of light was detected for each morphological type over the entire redshift range spanned by the data. In contrast, redshift surveys now routinely reach redshifts of 1 (e.g. CFRS, AUTOFIB; Lilly et al. 1995a, Ellis et al. 1996), such that even with a single limiting isophote, the fraction

of detected light for a galaxy is not the same at all redshifts. Furthermore, deep redshift surveys typically have much deeper limiting isophotes for both detection and photometry than do the local redshift surveys to which they compare, and typically do not make a correction onto a common isophotal magnitude limit. This discrepancy can lead to an apparent increase in the number density of galaxies with increasing redshift, as pointed out by McGaugh (1994), and explored in Ferguson & McGaugh (1995) and Phillipps & Driver (1995). Yoshii (1993) used similar techniques as will be outlined in this paper to calculate how the use of isophotal magnitudes affect the number counts and redshift distributions of faint galaxies.

In this paper, we investigate how biases resulting from the use of isophotal magnitudes affects the luminosity function in particular. We attempt to provide a guide for estimating the degree to which these biases may be present in different galaxy surveys. First, in §2, we outline the method for calculating the true volume of a galaxy survey using the fraction of observed light as a function of redshift, which we calculate in §3 as a function of observational parameters and intrinsic galaxy properties. We quantify the degree to which this will produce misestimates of the luminosity function, such that one can identify the observational regimes where these effects are not important. In §4 we use artificial galaxy catalogs to demonstrate how the measured luminosity function varies when different reconstructions of the luminosity function are used. In §5, we discuss ways in which the distribution of V/V_{max} can be used to test for the presence of luminosity function biases and in §6, we discuss the merits and drawbacks of alternatives to isophotal magnitudes.

2. V_{max} for Extended Objects

Measurements of the field luminosity function begin by calculating an absolute magnitude for each galaxy in a redshift survey, using

$$M = m - 25 - 5 \log \left(\frac{D_L(z)}{\text{Mpc}} \right) - 2.5 \log k(z), \quad (1)$$

where m is the apparent magnitude of an observed galaxy at redshift z , $D_L(z)$ is the luminosity distance appropriate for the chosen cosmology and $k(z)$ is the k -correction, which incorporates changes in magnitude due to the stretching of the bandpass and the variation in the observed rest-frame wavelength with redshift.

The relationship between apparent magnitude and absolute magnitude given in equation 1 is only correct in the limit where the apparent magnitude m is an accurate measure of the total flux, regardless of redshift or morphological type. More typically, however, the apparent magnitude which is used is either an isophotal magnitude (e.g. Lilly et al. 1995b, Ellis et al. 1996, Lin et al. 1996), a “total” magnitude measured within some multiple of the isophotal area (Small et al. 1997), a modified Kron (1980) magnitude measured within an aperture whose size is determined by the first moment radius of the light visible above some limiting isophote (Yee et al. 1996, Lin et al. 1997) or, more rarely, an aperture magnitude (Gardner et al. 1996, Glazebrook et al. 1994); we will restrict ourselves to the case of isophotal magnitudes for the purposes of this paper, since isophotal magnitudes are most commonly used, and other magnitude measures reduce to this case; we will consider alternative measures of magnitude in §6.

For an isophotal magnitude measured within a limiting isophote μ_{lim} , some fraction of the light is lost outside the outer isophote. The fraction of detected light, $f(z)$, depends both upon intrinsic properties of the galaxy (such as the intrinsic central surface brightness μ_0 , the true absolute magnitude M , the two-dimensional shape of the galaxy in the absence of seeing (i.e. its light profile)), as well as observational

parameters of the survey, such as the limiting isophote μ_{lim} and the point spread function.

The fraction of detected light also depends upon the redshift of the observed galaxy. As a galaxy moves to higher redshifts, it suffers two effects which rapidly decreases the fraction of light detected within a fixed isophotal limit. First, at large enough redshifts the galaxy appears small compared to the point spread function, and begins to lose light beyond the limiting isophote, due to the rapid falloff in the point spread function with radius. Second, the apparent surface brightness drops off as $(1+z)^{-4}$ due to the difference in the redshift dependences of the angular diameter and luminosity distances. As the drop in apparent surface brightness becomes significant (a factor of 2 at $z = 0.2$), a larger fraction of a galaxy’s light falls below the limiting isophote, again increasing the fraction of lost light. The direction of both of these effects is for the apparent magnitude to drop off more quickly with distance than predicted by equation 1.

If instead, one includes the correction for lost light, equation 1 becomes

$$M = m_{iso} - 25 + 2.5 \log f(z) - 5 \log \left(\frac{D_L(z)}{\text{Mpc}} \right) - 2.5 \log k(z). \quad (2)$$

Including the fraction of detected light $f(z)$ has two effects. First, because $f < 1$, the absolute magnitude of each galaxy is calculated to be brighter, which compensates for the unobserved light beyond the limiting isophote. Second, when equation 2 is inverted to find the maximum redshift at which the galaxy would be included in the sample (i.e. z_{max} such that $m_{iso} = m_{lim}$), then the effective luminosity distance is increased, and thus a smaller z_{max} is derived than in the absence of the lost light term. This reduces the maximum volume V_{max} , which in turn increases the derived luminosity density (which scales with $1/V_{max}$).

In luminosity function calculations which reduce the effects of spatial inhomogeneities (Sandage et al. 1979, Efstathiou et al. 1988), the derived luminosity function depends upon maximizing the likelihood $\ln \mathcal{L}_i = \ln \phi(M_i) - \ln \int_{M_{max}(z_i)}^{M_{max}(z_i)} \phi(M) dM$, summed over all galaxies in the survey. For these derivations, including the lost light in equation 2 reduces the range of possible M , which will change the shape of the luminosity function. The normalization of the luminosity function in these methods, like the classical methods, depends upon the sum of $1/V_{max}$, and will also be higher when the effects of lost light are included.

3. Calculating the Observed Light Fraction $f(z)$

Given equation 2 for the relationship between absolute magnitude and apparent isophotal magnitude as a function of redshift, it is in principle straightforward to calculate the luminosity function for a given sample. The reconstructions of the luminosity function which are currently in use can readily be applied, but with the substitution of the correct values of z_{max} , or with the correct range of absolute magnitudes at a given redshift.

The difficulty in calculating the luminosity function becomes calculating the form of $f(z)$ for the galaxies within a sample. For a galaxy with a fully specified two-dimensional surface brightness profile, one can calculate $f(z)$ at any redshift by first rescaling the central surface brightness by $(1+z)^{-4}$ and applying the k -correction, then calculating the angular size using the angular diameter distance, and finally convolving the resulting 2-d angular light distribution with the point spread function. Then, $f(z)$ may be calculated by integrating the resulting light distribution over the area where the surface brightness is greater than the limiting isophote μ_{lim} , or within an area appropriate to any other magnitude measure.

There are several existing papers which calculate the fraction of detected light $f(z)$, particularly in the case of large photographic surveys wherein image saturation is important but seeing can be neglected. Disney & Phillipps (1983) have calculated $f(z)$ for circular axisymmetric galaxies with both exponential and de Vaucouleurs profiles, and used the resulting lost light fraction to calculate the relative V_{max} for galaxies of varying surface brightness, at fixed total luminosity³. Their analysis includes the effects of combined isophotal magnitude limits and angular diameter limits. Davies (1990) has expanded upon the work of Disney & Phillipps, by generalizing the calculation of the lost light and V_{max} to include combined bulge+disk models, and random inclinations.

The earlier work of Disney & Phillipps has also been extended to higher redshifts by Phillipps et al. (1990), who include the effect of cosmological dimming and k -corrections in calculating both the fraction of detected light and V_{max} as a function of intrinsic surface brightness and luminosity, for face-on exponential disks in the absence of seeing. Using a simple model, they demonstrate how failure to compensate for the variation in the effective survey volumes with variation in galaxy surface brightness can lead to underestimating the luminosity function for low surface brightness galaxies.

At moderate redshifts, however, seeing can be as important as surface brightness in modifying the fraction of observed light and biasing V_{max} . When the half-light radius of a galaxy approaches the size of the point spread function (PSF), the observed light profile becomes dominated by the PSF. This can become significant even at relatively moderate redshifts ($z \sim 0.1$). In a separate paper (Dalcanton 1998), we derive an analytic expression for the observed light fraction $f(z)$ of axisymmetric exponential disks and de Vaucouleurs profile ellipticals in the presence of a realistic Moffat (1969) point spread function, which we will use for the duration of this paper; Yoshii (1993) has calculated $f(z)$ for the simpler case of a Gaussian point spread function. We parameterize the two types of profiles with a characteristic surface brightness μ_0 and a length scale α . For the exponential profile, μ_0 is the central surface brightness, and α is the exponential scale length. For the de Vaucouleurs profile, we chose α and μ_0 such that the de Vaucouleurs galaxy has the same half light radius and total flux as an exponential galaxy with the same parameters. With this choice, $\mu_0 = \mu_e - 2.518$ and $\alpha = r_e/1.679$, where μ_e and r_e are the more typical parameterizations of the de Vaucouleurs profile.

Using the prescription in Dalcanton (1998), and neglecting the k -correction for generality, we have calculated the quantity $\Delta M(z) = -2.5 \log f(z)$, which characterizes the degree to which the apparent isophotal magnitude m falls off faster than $1/D_L^2(z)$. We have plotted $\Delta M(z)$ for different galaxy sizes (solid, dashed, and dotted lines) and characteristic surface brightnesses relative to the limiting isophote ($\Delta\mu = \mu_{lim} - \mu_0$ decreasing from left to right), and for variable seeing (increasing from top to bottom), for the cases of exponential (Fig. 1[a]) and de Vaucouleurs (Fig. 1[b]) light profiles. These plots can be used to identify the regimes where a survey may suffer from systematic biases in the measured the luminosity function; when $\Delta M(z)$ is large over a survey’s redshift range, the apparent magnitude of a galaxy can be much fainter than would be predicted by eqn. 1 alone, and thus, a given galaxy drops below some isophotal magnitude limit faster than predicted by eqn. 1.

For both types of galaxy profiles, the curves in Figure 1 show the expected behavior for $\Delta M(z)$. At low redshifts, $\Delta M(z)$ is constant, because the fraction of lost light does not change dramatically with increasing distance. When the redshift becomes large enough, however, a given galaxy becomes small with respect to

³The relative V_{max} as a function of surface brightness, luminosity, and/or scale length is sometimes referred to as the “visibility” in the literature (e.g. Disney & Phillipps 1983), since it reflects the relative contribution of different galaxies to a given survey. Thus, galaxies which have a smaller V_{max} are less likely to appear in a survey, and are thus less “visible”

the point-spread function, and, if the redshift approaches 1, the apparent surface brightness drops rapidly due to the $(1+z)^{-4}$ surface brightness dimming. These two effects drop the apparent flux precipitously, increasing $\Delta M(z)$.

At low redshifts, where $\Delta M(z)$ is constant, the apparent magnitude falls off as expected by eqn 1, and thus, as long as the maximum redshift reached by a survey falls within this flat regime, the standard reconstruction of the luminosity function is valid (i.e. eqn. 1)⁴. In contrast, if the limiting magnitude of a survey is very faint, then a significant fraction of galaxies will be at large enough redshifts that $\Delta M(z)$ is not constant over the survey volume. In this case, the apparent magnitude will be falling faster than expected, and thus the luminosity function will be systematically underestimated. In particular and perhaps counterintuitively, the luminosity function is more likely to be underestimated in the bright end, since these galaxies will be detectable over the largest range in redshift. On the other hand, the redshift at which $\Delta M(z)$ becomes large is smallest for intrinsically small galaxies, and for low surface brightnesses galaxies. Thus, in deep enough surveys, the luminosity function may be biased in the faint end. The error in the derived luminosity function will also depend upon the characteristic redshift of the survey, and thus, the luminosity function calculated for the same type of galaxies can be quite different from survey to survey, due to variations in the maximum redshift explored by a survey (i.e. m_{lim}), variations in the seeing, or variations in the limiting isophote μ_{lim} .

Even in the case of optimal seeing, where $\Delta M(z)$ is constant over a large redshift range, there can be large effects on the derived luminosity function. As seen in Figure 1, when a galaxy’s central surface brightness approaches the limiting isophote, there is a global offset in $\Delta M(z)$, which increases as the surface brightness decreases. This offset leads low surface brightness galaxies to have systematically underestimated luminosities (see discussions by Disney 1976, Disney & Phillipps 1983, for example), even in the absence of seeing effects. Thus, only the very nearest low surface brightness galaxies will be bright enough to be within the magnitude limit of a survey, and as such, LSBs have much lower detection volumes, even at low redshifts where $\Delta M(z)$ is constant; this argument has been framed as the classic “visibility” problem by Disney (1976), Disney & Phillipps (1983), Davies (1990), & McGaugh et al. (1995). Furthermore, if surface brightness is correlated with absolute magnitude, as seen in clusters of galaxies (e.g. Binggeli et al. 1984), then the underestimate of the luminosity becomes increasingly severe at faint absolute magnitudes. This correlation would produce a stretching of the luminosity function, which in turn would lead to a smaller faint end slope. The effect is nearly independent of seeing, and has been discussed by Phillips et al. (1990).

Figure 1 also reinforces the value of having very deep, high-resolution imaging data when selecting targets for a redshift survey, such that the magnitude limit of the survey is many magnitudes above the limiting magnitude of the imaging data. For such cases, the vast majority of galaxies will have limiting isophotes for both detection and photometry which are well below their central surface brightness, and as Figure 1 shows, such surveys will have far fewer problems with isophotal magnitude biases, as they will contain a very large fraction of most galaxies’ light out to $z \sim 1$.

Finally, to give some appreciation for the values of $\Delta\mu = \mu_{lim} - \mu_0$ and α which might be applicable for typical surveys, Figure 2 shows μ_0 and α derived from surface photometry for an assortment of galaxy samples, chosen to be representative of the range of galaxy morphologies and luminosities (and not to be a definitive compilation on galaxy structural parameters). Bright ellipticals tend to have $21 < \mu_0 < 18 B \text{ mag/arcsec}^2$, while spirals have $\mu_0 > 20 B \text{ mag/arcsec}^2$, down to the current surface

⁴For example, if one were calculating the luminosity function for high surface brightness galaxies selected from HST imaging (e.g. upper left in Figure 1), the reconstructed luminosity function would be valid for all redshifts less than 1.

brightness limits of major surveys ($\mu_0 \sim 24 B \text{ mag/arcsec}^2$). Bulges tend to have the highest surface brightnesses ($15 < \mu_0 < 21 B \text{ mag/arcsec}^2$), but also tend to be factors of 10 smaller than ellipticals and spirals. However, the lack of small spirals with $\alpha < 1 h_{50}^{-1} \text{ kpc}$ is an artifact of only plotting spirals drawn from angular diameter limited surveys, which are strongly biased towards identifying galaxies with large physical sizes. We also note that, because of k -corrections and evolutionary effects, the appropriate value of μ_0 can be a strong function of redshift; for example, while elliptical galaxies might have $\Delta\mu = 5$ in blue bandpasses at low redshift, a value of $\Delta\mu = 1$ may be more appropriate at redshifts close to 1. There are fewer surface photometry measurements available for other band passes, but for reference, the equivalent to the Freeman (1970) surface brightness is $20.1 \text{ mag/arcsec}^2$ in r , and $\sim 17.6 \text{ mag/arcsec}^2$ in K for galactic disks (Courteau 1996, de Jong 1996b).

To derive $\Delta\mu$, the surface photometry presented in Figure 2 can be compared with the isophotal limits for recent field surveys, which we have attempted to summarize in Table 1. The Table is provided only as a rough guide, given that in many cases, the photometric selection criteria are complicated and/or not fully specified, and the reader should refer to the original papers for a more complete description. For many of the entries we have estimated the limiting surface brightness for detection based upon the given photometric limits, or measures of the sky noise, where possible; only the CFRS and Norris surveys have adequately tested this limit using realistic artificial galaxy tests. An examination of Table 1 shows that the best infrared field surveys to date have only $\Delta\mu \lesssim 1.5$ for pure spiral disks, suggesting that the current generation of K band luminosity functions reflect the properties of the high surface brightness elliptical population alone.

4. Luminosity Functions

The above results suggest that the measured luminosity function can depend sensitively upon the survey used to select galaxies, and upon the redshifts and morphologies of the galaxies which have been selected. In this section we explore in more detail the specific ways in which the luminosity function may be affected, by simulating the entire process of measuring a luminosity function, including both sample selection and standard reconstructions of the luminosity function. For this exercise, we will neglect spatial density inhomogeneities, and use the “classical” $1/V_{max}$ calculation for deriving the luminosity function; more sophisticated maximum-likelihood methods should produce identical results in the limit of smooth galaxy distributions.

In general, reconstruction of the luminosity function proceeds as follows:

Step 1. A sample of galaxies whose apparent magnitude m is above some threshold m_{lim} is selected. There may also be additional selections for apparent angular size, particularly for nearby photographic surveys. Size criteria will be neglected for the following exercise.

Step 2. Redshifts are measured for the selected galaxies, and, when combined with the apparent magnitudes m , are used to derive absolute magnitudes using equation 1.

Step 3. The maximum redshift possible for each galaxy is calculated by solving equation 1 for z_{max} , using the derived absolute magnitude from Step 2, and assuming $m = m_{lim}$.

Step 4. The volume V within z_{max} is calculated for each galaxy, and then the inverse is summed over all galaxies within absolute magnitude bins, to derive the relative number density as a function of absolute magnitude.

There are two competing effects which can affect the galaxy luminosity function derived with the standard methods. First, due to the lost-light beyond the outer isophote, galaxies will have systematically fainter derived absolute magnitudes, because Step 2 assumes that the observed magnitude m is a good representation of the total flux from a galaxy. Then, when the artificially faint absolute magnitude is used to calculate z_{max} in Step 3, one will estimate that the galaxy has a smaller maximum redshift than if all the light were included in the measurement of m . This leads one to underpredict the maximum volume V_{max} , and thus calculate larger values of the luminosity function in Step 4. One will also calculate larger values of V/V_{max} for galaxies which are strongly affected by this bias. The second effect works in the opposite sense. As shown in §3, due to the variation in the fraction of detected light $f(z)$ with redshift, a galaxy’s apparent magnitude can fall off much faster with redshift than predicted by equation 1 alone (i.e. eqn. 2). This leads one to overpredict the maximum redshift, and thus underpredict the luminosity function. In this case, the derived values of V/V_{max} will be smaller than expected. Because these two effects compete with each other, it is possible for a sample to have $\langle V/V_{max} \rangle \sim 0.5$, in spite of the measured luminosity function being strongly distorted from the true underlying distribution.

To demonstrate the size of these effects, we have modelled the case of a moderately deep redshift survey in Figure 3, for the specific case of a limiting isophotal magnitude of $m_{lim} = 22$ within a limiting isophote of $\mu_{lim} = 25 \text{ mag/arcsec}^2$, for galaxies with different characteristic surface brightnesses, and for both exponential and de Vaucouleurs light profiles. The analysis assumes that one is calculating the full bivariate luminosity function⁵, where the galaxies are binned not only in luminosity, but also in intrinsic surface brightness μ_0 .

To create a simulated galaxy sample, we have populated a universe with a uniform density of face-on galaxies of a fixed characteristic surface brightness, drawn randomly from a Schechter (1976) luminosity function $\Phi(M)$ with $M_* = -21$ and $\alpha_{lum} = -1.5$. Note that the choice of M and μ_0 fixes the exponential scale length, such that variation in M at fixed surface brightness is effectively a variation in size. This is a reasonable approach for spiral disks, which span a continuous range of μ_0 and α , but is somewhat artificial for pure elliptical galaxies, which tend to fall along a locus in μ_0 vs α (Figure 2). We retain this choice for ellipticals, however, because it more clearly elucidates the general trends which are expected, and because, in general, a bivariate luminosity function will probably not further subdivide a luminosity function by profile shape, in addition to surface brightness. For each surface brightness, we calculate the observed isophotal magnitude using Moffat convolved galaxy profiles and generate a catalog of 5,000 galaxies which fall above the isophotal magnitude limit. The resulting catalog is then analyzed using the methods most typically applied to galaxy catalogs (Steps 1-4 above; eqn. 1), and then reanalyzed using the proper correction for lost light (eqn. 2). For the sake of generality, we have neglected the k -correction term in eqn. 2, both in generating the catalog and in analyzing it; we will discuss the role of the k -correction below. The final luminosity function and V/V_{max} distributions are shown in Figure 3.

There are several obvious trends demonstrated in the luminosity functions plotted in Figure 3:

1. As expected from Figure 1, the errors in the derived luminosity function are greater for low surface brightness galaxies, due to the increased fraction of lost light, and the lower redshift at which $\Delta M(z)$ becomes large. The biases are slight when the characteristic surface brightness μ_0 is 5 mag/arcsec^2 above

⁵This has also been referred to as the bivariate brightness function (BBF) by Phillipps et al. (1990) and Boyce & Phillipps (1995). We prefer to retain the phrase “luminosity function”, to maintain the analogy to previous work on the galaxy luminosity function. See Boyce & Phillipps (1995) for a good discussion of the elements necessary to a survey designed to measure the full bivariate luminosity function

the limiting magnitude, significant at $\Delta\mu = 3 \text{ mag/arcsec}^2$, and severe at $\Delta\mu = 1 \text{ mag/arcsec}^2$ (where $\Delta\mu = \mu_{lim} - \mu_0$).

2. The underestimate in the luminosity function is worse at high redshift, due to the rapid variation in the lost light fraction at increasing redshift. Furthermore, in low-redshift subsamples, some portion of the sample has V_{max} fixed by the upper cutoff in redshift, which reduces the impact of ignoring the lost light corrections. This suggests that when the luminosity function is derived in intervals of redshift, evolution detected in the luminosity function may be correct for the lower redshift intervals, but evolution between the penultimate and the highest redshift interval is suspect.

3. The underestimate of the luminosity function is worse at bright magnitudes, as these galaxies tend to be at larger redshifts, where the light lost fraction changes rapidly.

4. The luminosity functions appear to shift to fainter M_* with decreasing surface brightness, due to the increasing offset in $\Delta M(z)$ (see Figure 1).

5. The mismeasurement of the luminosity function can mimic luminosity and density evolution. The luminosity function appears to shift towards brighter magnitudes and to larger normalizations as the redshift decreases (see the comparison between the dotted and solid curves in the lower left panels of Figure 3). Including k -corrections and evolutionary corrections can induce the opposite effect. Most galaxies are probably intrinsically brighter at higher redshifts, and thus the appropriate value of $\Delta\mu_0$ may be larger with increasing redshift, if the evolutionary corrections are larger than the k -corrections (as might be the case for galaxies with an exponentially declining star-formation rate). The luminosity function will then shift to higher luminosities at larger redshifts due solely to biases, and will therefore have the appearance of more rapid luminosity evolution than is the case.

6. For samples with the same number of galaxies, the underlying luminosity function has a much higher normalization for low surface brightness galaxies, due to their smaller mean distance in isophotal magnitude limited surveys; note the difference in the mean redshift as the surface brightness is decreased. This is the classical “visibility” effect discussed by Disney (1976), Disney & Phillips (1983), Davies (1980), McGaugh et al. (1995), and others. The relative normalizations of the luminosity functions suggest that galaxies with $\Delta\mu = 1 \text{ mag/arcsec}^2$ will be underrepresented by a factor of 10, compared to a population of galaxies with an identical space density and $\Delta\mu = 5 \text{ mag/arcsec}^2$. If the lower surface brightness galaxies are not treated separately, then the derived luminosity function will be 10% higher than would be correct for $\Delta\mu = 5 \text{ mag/arcsec}^2$, but will be a factor of 10 smaller than is correct for the entire surface brightness range spanned by the sample ($\Delta\mu > 1 \text{ mag/arcsec}^2$). In such instances, one should quote that the derived luminosity function is representative of only the high surface brightness fraction of the sample, even if the survey is capable of reliably detecting galaxies at much lower surface brightnesses.

7. At the same surface brightness, the mismeasurement of the luminosity function is comparable for both exponential and de Vaucouleurs profiles, as would be expected by the general similarity of the detected light fraction $f(z)$ plotted in Figure 1. However, ellipticals and bulges have somewhat higher surface brightnesses than spiral disks (Figure 2), by about $1\text{-}2 \text{ mag/arcsec}^2$ at the bright end, and thus ellipticals and early type spirals will tend to be less affected by luminosity function biases, when the k -correction is negligible. In contrast, Figure 2 also shows that ellipticals and spirals have comparable half-light radii, and thus both types of galaxies will begin to be affected by seeing at similar redshifts. Bulges have much smaller half-light radii than their spiral hosts, and while a high surface brightness bulge will help a spiral galaxy’s detectability, at redshifts $z \gtrsim 0.1$ the bulge profiles begin to be strongly affected by seeing for typical ground based observations. As a result, bulges may tend to become undetectable at comparable

redshifts as their associated disks (e.g. compare the tracks in Figure 1[b] for $\Delta\mu = 7$ and $\alpha = 0.25$ kpc to the tracks in Figure 1[a] for $\Delta\mu = 3$ and $\alpha = 3$ kpc).

8. There is less appearance of “evolution” for the de Vaucouleurs profiles than for the exponentials, in the absence of the k -correction, because $f(z)$ is constant over a slightly larger range in redshift for the de Vaucouleurs profile, while having a sharper increase at high redshift, and because $f(z)$ varies more strongly with surface brightness in exponential disks than in de Vaucouleurs ellipticals. These effects also lead to ellipticals having smaller mean redshifts than comparable spirals at high surface brightnesses ($\Delta\mu > 3$) and larger mean redshifts at low surface brightnesses ($\Delta\mu \leq 1$).

5. V/V_{max} Distributions

The degree to which the luminosity functions seen in Figure 3 have systematic problems can be partially diagnosed using the derived V/V_{max} distributions. As presented in Figure 3, as the corrections for lost light become larger (i.e. at lower central surface brightnesses and higher redshifts) the distributions of V/V_{max} become sloped, such that the distributions are elevated at small values of V/V_{max} and are depressed at larger values. The nature of the deformation is such that it nearly preserves the expectation value of $\langle V/V_{max} \rangle = 0.5$, even in the presence of severe problems in the derivation of the luminosity function. Thus, the full distribution of V/V_{max} is needed to test for the presence of lost-light biases. In the presence of the necessary k -correction, however, the full V/V_{max} distribution may well deviate from the relatively straight line seen in Figure 3, and pull the mean $\langle V/V_{max} \rangle$ from its expected value of 0.5.

Ideally, the V/V_{max} test should be performed in several redshift bins, given that the low redshift subsample of the $\Delta\mu = 1$ mag/arcsec² sample is clearly biased in its luminosity function derivation, while having a nearly normal V/V_{max} distribution. This apparent normality results from V_{max} being fixed by the upper cutoff in redshift for a large fraction of the galaxies. In general, the slope in the V/V_{max} distribution is somewhat more severe for disk galaxies than comparable elliptical galaxies.

We note that the expected signature has already been seen in the data used for the Autofib survey (Ellis et al. 1996; their Figure 2). Even after correction for redshift incompleteness, their published V/V_{max} distributions systematically fall off towards large values of V/V_{max} , and look remarkably similar to the plots in Figure 3. Most other existing surveys have published only the mean $\langle V/V_{max} \rangle$ and cannot be immediately tested for the biases discussed here.

6. Alternative Measures of Luminosity

The systematic biases in the luminosity functions presented in Figure 3 are a direct result of the practice of using isophotal magnitudes to measure galaxies’ luminosities. There are other ways to measure galaxy magnitudes however, which, while less commonly used, can potentially improve the accuracy of the luminosity function reconstruction.

The easiest alternative to the isophotal magnitude is the aperture magnitude. One can choose a large enough aperture to safely contain a large fraction of a typical galaxy’s light, and thus have a measure of the total luminosity which is not biased with surface brightness. However, aperture magnitudes are strongly biased with galaxy size; physically large galaxies will have a smaller fraction of their light detected than will smaller galaxies, leading the brighter galaxies to be measured with a smaller intrinsic luminosity. The

degree of mismeasurement will also be a function of redshift, with a larger fraction of a galaxies’ light being detected at higher redshift. This redshift dependence is opposite to the behavior of isophotal magnitudes, as can be seen in the top row of Figure 5, where we have plotted the error in the measured absolute magnitude as a function of redshift, for a 3’’ diameter aperture (as in Lilly et al. 1991, for 1’’ seeing), applied to various galaxy profiles and physical sizes. Because it is the redshift dependence of ΔM which led to the artificial appearance of galaxy evolution in Figure 3, aperture magnitudes should also produce artificial evolution, although with the opposite luminosity evolution. As can be seen from Figure 5, even for a large aperture ($3\times\text{FWHM}$), a typical spiral with $\alpha = 3\text{ kpc}$ is biased by over 1 magnitude at $z = 0.1$.

Another common practice is to attempt to correct a measured isophotal magnitude to a “total” magnitude. The “total” magnitudes provided by the FOCAS package (Valdes 1982) are created by extending the isophotal area by a factor of 2, and then measuring the flux within the larger aperture. While not immediately apparent, the FOCAS “total” magnitudes are actually equivalent to an isophotal magnitude measured at a fainter limiting isophote. Thus, one can consider using a FOCAS “total” magnitude as increasing the value of $\Delta\mu = \mu_{lim} - \mu_0$, where μ_{lim} is the limiting isophote for the initial detection of the galaxy. For pure exponentials, the new effective magnitude difference is always $\Delta\mu_{eff} = \sqrt{A}\Delta\mu$, where A is the factor by which the isophotal area is grown. For pure de Vaucouleurs profiles, $\Delta\mu_{eff} = A^{1/8}\Delta\mu + 5.81(A^{1/8} - 1)$, and for galaxies which are small enough to have nearly Gaussian profiles due to the seeing, $\Delta\mu_{eff} = A\Delta\mu - 5(A - 1)\log\sigma/\alpha$, where σ is the standard deviation of the Gaussian point spread function, and α is the galaxy’s scale length. Because the increase in $\Delta\mu_{eff}$ is largely a multiple of the isophotal value of $\Delta\mu$, changing from an isophotal magnitude to a “total” magnitude does not greatly reduce the level of systematic bias for lower surface brightness galaxies; a galaxy with $\Delta\mu = 1.5$ has $\Delta\mu_{eff} = 1.5 - 2.1$ when FOCAS “total” magnitudes are used.

There are other forms of “total” magnitudes, besides those used by FOCAS. One of the most common of these is the Kron (1980) magnitude, which sets the aperture to be a multiple of the intensity-weighted first moment radius r_1 , instead of a multiple of the isophotal area. With careful consideration of the effects of seeing, the Kron magnitude can provide a fairly robust method of providing a magnitude measurement which is consistent over a range in redshifts and observing conditions (see Bershady et al. 1994 for a particularly cogent discussion of the relevant issues). The consistency of the Kron magnitude with variations in surface brightness has not yet been sufficiently explored, however. Galaxies whose apparent central surface brightness approaches the isophotal limit are typically detected out to only one scale length, and thus will tend to give systematically smaller values of r_1 ; the degree of this mismeasurement will depend sensitively on the details of how r_1 is measured (iteratively, directly, etc).

We test the sensitivity of Kron magnitudes to variations in surface brightness in Figure 4, where we have assumed that r_1 is measured above some limiting isophote μ_{lim} , and that the Kron magnitude is calculated within a radius $r_{ap} = 2r_1$, as suggested in Kron (1980). Figure 4 shows that the Kron magnitude underestimates the total luminosity at low surface brightnesses ($\mu_{lim} - \mu_0 \lesssim 3$), much like isophotal magnitudes do. For $\Delta\mu \sim 3$, errors in the absolute magnitude are larger than $0.3 - 0.7^m$, and increase in size towards fainter surface brightnesses (i.e. smaller $\Delta\mu$). The errors at low surface brightnesses are also larger when the PSF dominates the galaxy profile. The curves shown in Figure 4 are actually worst case scenarios, as we do not calculate r_1 iteratively, nor do we prevent the Kron radius $2r_1$ from becoming smaller than either some multiple of the original limiting isophotal radius or some fixed aperture radius, both of which will give better estimates of the total magnitude than given in Figure 4. However, as in the case of FOCAS total magnitudes, calculating r_1 iteratively is equivalent to using a fainter value of μ_{lim} , and thus a somewhat larger value of $\Delta\mu$. The curves in Figure 4 will therefore be identical when iterative

measures of r_1 are used, but the appropriate value of $\Delta\mu$ will be larger. The situation is similar when there is a minimum allowed Kron radius, if the minimum radius is set to be a multiple of the original limiting isophotal radius (as in SExtractor, Bertin & Arnouts 1996). If the minimum Kron radius is a fixed aperture, then the biases for the faintest galaxies will become those suffered by aperture magnitudes.

Another alternative to either the isophotal or aperture magnitude is the Petrosian magnitude (1976). To define a Petrosian magnitude, one fixes the value of the parameter η , finds the Petrosian radius where $\eta = \langle \Sigma(r) \rangle / \Sigma(r)$, and then measures the flux within that radius (here, $\langle \Sigma(r) \rangle$ is the mean surface brightness within r). Because the characteristic surface brightness cancels in the definition of η , the Petrosian radius will be identical for galaxies with the same profile shape, independent of their surface brightness, and thus the fraction of detected light $f(r)$ will be constant with surface brightness as well. Furthermore, unlike for aperture magnitudes, the fraction of a galaxy’s luminosity contained within the Petrosian radius is independent of a galaxy’s size or distance, and depends only upon the particular choice of η , and the shape of the galaxy’s profile (in the absence of seeing). These qualities make the Petrosian magnitude a nearly ideal choice for measuring luminosity functions in a way that is unbiased with redshift or surface brightness. The stability of the Petrosian magnitude can be seen in the bottom of Figure 5. The Petrosian absolute magnitude is nearly constant with redshift for pure exponential disks of different sizes, even when a $1''$ PSF is included. For de Vaucouleurs profiles, the absolute magnitude varies by only 0.2 magnitudes out to a redshift of 2, and differs from exponential profiles by roughly the same amount. We have chosen the value of η carefully, to give a good compromise between including a large fraction of a galaxy’s light, yielding consistent results for elliptical and spiral profiles, and producing small enough Petrosian radii that $\Sigma(r)$ can be accurately measured; for different choices of η , the results in Figure 5 could be very different. The comparison of exponential profiles to de Vaucouleurs profiles in Figure 5 suggests that even for a realistic mixture of galaxies, Petrosian magnitudes should be able to make consistent measures of luminosity over a large range in galaxy size, surface brightness, and redshift, leading to a vast improvement over the standard use of isophotal magnitudes.

While Petrosian magnitudes appear to offer a nearly ideal tool for measuring galaxy luminosities, the plots in Figure 5 disguise several difficulties. In general, Petrosian magnitudes are subject to large errors at low signal-to-noise ratios and for poorly sampled profiles. To find the radius corresponding to a particular value of η in a faint galaxy image, one must carefully interpolate over a relatively small number of pixels to find r , $\Sigma(r)$ and $\langle \Sigma(r) \rangle$. For low surface brightness galaxies or normal galaxies at moderate redshifts, the particular value of η may require accurately measuring extremely faint surface brightnesses (i.e. $\mu_0 \sim 30$ mag/arcsec²), which may be well beyond the capabilities of the available imaging data, due to sky noise, flat-fielding, crowding, etc. Thus, while Figure 5 suggests that Petrosian magnitudes are unbiased with surface brightness or size in ideal data, for noisy, binned data, there should be both noise and systematic biases which will get worse with decreasing surface brightness and redshift, although hopefully to a lesser degree than isophotal magnitudes.

Wirth (1996) has explored the systematic errors in Petrosian magnitudes for different interpolation schemes, and for different signal-to-noise ratios. He finds that the simplest interpolation methods are highly biased with signal-to-noise, and while more sophisticated ones can be constructed, they are only useful for galaxies which have a signal-to-noise ratio above 10 within their true half-light radii. At $\text{SNR}_{0.5} = 10$, the best estimators have a typical scatter in the Petrosian radius of more than 50%, and a systematic bias of about 30%, which will translate into systematic errors and increased scatter in the measured Petrosian magnitudes for faint galaxies. The simplest interpolation schemes produce much larger systematic biases, which reach over 80% in the Petrosian radius at $\text{SNR}_{0.5} = 10$. Because of these systematics, the robustness

of any adopted scheme for measuring Petrosian magnitudes should be thoroughly tested as a function of surface brightness, size, and signal-to-noise, before they can be safely invoked as a panacea for the problems which can plague isophotal magnitude determinations of the luminosity function.

Wirth (1996) also finds that for galaxies with high signal-to-noise ($\text{SNR}_{0.5} \sim 80$), the measured Petrosian radii are good to within 10% which suggests that one could perform a nearly ideal luminosity function reconstruction for deep enough imaging data. However, even the best data is subject to the strong isophotal magnitude biases discussed in the rest of this paper. The detection of galaxies is fundamentally an isophotal signal-to-noise limited process; one will never measure photometry for a galaxy which does not have substantial light above the sky noise of a given image. Thus, all surveys have an implicit isophotal magnitude limit, which is roughly the standard completeness limit of a survey. In determining the biases in a luminosity function measurement, even if using Petrosian magnitudes, one must also consider the impact of the implicit isophotal magnitude limit as well.

7. Conclusions and Complications

In the current epoch of deep CCD imaging, some surveys have extended into a redshift regime where the light lost beyond the outer detection isophote, due to intrinsic surface brightness and seeing, can have large, systematic effects upon the derived luminosity function, without violating the standard $\langle V/V_{max} \rangle$ tests which are often used to diagnose incompleteness and unusual systematics. We have attempted to give a general guide to determining the regimes where corrections for lost light become important, and to estimating the degree to which neglecting the corrections can affect the resulting luminosity function. We have also shown how these effects can easily mimic evolution in the galaxy population. As an aside, we note that the biases we discuss are potentially relevant to any work which involves detection of extended objects, such as the detection of galaxy clusters in X-ray data.

In our investigation, we have taken the simplest, most general assumptions, in order to clarify the general biases which affect luminosity function measurements, and to estimate the size of these biases in different regimes. This approach comes at the expense of glossing over some subtleties which can affect real surveys. Perhaps the most glaring complication is that in many surveys, the limiting isophote for detection is substantially brighter than the limiting isophote for photometry. For example, the CFRS survey (Lilly et al. 1995a) uses a very deep isophotal limit of roughly $\mu_{IAB} = 28.5$ for photometry (which guarantees that they measure a consistently large fraction of a detected galaxy’s light), but has an effective isophotal limit for detection of roughly $\mu_{IAB} \sim 25.5$ (estimated from the central surface brightness detection limit in their Figure 2), due to sky noise and flat-fielding uncertainties. In such cases, one must take additional care in calculating V_{max} , such that the maximum redshift is derived with the additional criteria that the object can be detected above the limiting isophote for detection, as well as having an isophotal magnitude brighter than the limiting magnitude of the survey. Testing for a galaxy’s detectability is further complicated by the usual practice of smoothing an image before searching for galaxies within it. For imaging data which is substantially deeper than the limiting magnitude of the spectroscopic subsample, many of these problems can be avoided.

For simplicity, we have also neglected the mix of complicated morphologies and viewing angles present in the real universe, and instead used face-on circularly symmetric exponential disks and de Vaucouleurs profile ellipticals for illustration. As almost all galaxies can be reasonably approximated by a sum of the two profile types, reality is likely to be bracketed by these two limiting cases. If a survey is in a redshift

regime or a surface brightness regime where the corrections for lost light are probably large (see Figure 1), then the optimal method for deriving V_{max} is to first fit an inclined bulge/disk model to each galaxy, then to calculate V_{max} by simulating the individual galaxies as they would be observed at higher redshifts (including the likely k -corrections), using either analytic calculations or artificial galaxy tests. In the latter case, one can readily incorporate the complications of galaxy detection as a function of redshift, as well as the effects upon the photometry. We have also shown how the use of Petrosian magnitudes can greatly reduce the size of the needed corrections, but have argued that their benefits are most substantial at relatively high signal-to-noise ratios.

While making these further corrections can be a fair bit of work, and will certainly be subject to their own errors and biases, for the typical size of galaxy surveys ($\lesssim 1000$ galaxies) such an approach is not necessarily untenable, and for larger galaxy surveys, such as the upcoming 2DF and Sloan surveys, this can be approached in a binned, statistical way, and/or can be heavily automated. Many groups have already implemented routines to estimate structural parameters for galaxies using deconvolution and/or maximum likelihood methods (e.g. Schade et al. 1996, Ratnatunga et al. 1994), and from there, it is a small extrapolation to calculate the correct V_{max} . At the least, it is preferable to make a first-order correction when needed, than to ignore effects which may be large enough to obscure the cosmology that one is hoping to illuminate.

Acknowledgements

It is a pleasure to thank Rebecca Bernstein for sage council during the course of this work, Steve Shectman for his services as a sounding board in the early stages, Dan Rosenthal for shrewd discussions, and John Mulchaey for the tireless efforts of his workstation. An anonymous referee is also thanked for many helpful suggestions. Support was provided by NASA through Hubble Fellowship grant #2-6649 awarded by the Space Telescope Science Institute, which is operated by the Association of Universities for Research in Astronomy, Inc., for NASA under contract NAS 5-26555.

8. References

- Arp, H. 1965, *Ap. J.*, 142, 402.
- Bershady, M. A., Hereld, M., Kron, R. G., Koo, D. C., Munn, J. A., & Majewski, S. R. 1994, *A. J.*, 108, 870.
- Bertin, E., & Arnouts, S. 1996, *Astr. Ap. Suppl.*, 117, 393.
- Binggeli, B., Sandage, A., & Tammann, G. A. 1988, *Ann. Rev. Astr. Ap.*, 26, 509.
- Binggeli, B., Sandage, A., & Tammann, G. A. 1984, *A. J.*, 89, 64.
- Boroson, T. 1981, *Ap. J. Suppl.*, 46, 177.
- Boyce, P. J., & Phillipps, S. 1995, *Astr. Ap.*, 296, 26.
- Caldwell, N., Armandroff, T. E., Seitzer, P., & Da Costa, G. S., 1992 *A. J.*, 103, 840.
- Courteau, S., 1996, *Ap. J. Suppl.*, 103, 363.
- Dalcanton, J. J. 1998, *A. J.*, submitted.

- Davies, J. I. 1990, M.N.R.A.S., 244, 8.
- de Jong, R. S., 1996a, Astr. Ap. Suppl., , 118, 557.
- de Jong, R. S., 1996b, Astr. Ap., , 313, 45.
- Disney, M. 1976, Nature, 263, 573.
- Disney, M., & Phillipps, S. 1983, M.N.R.A.S., 205, 1253.
- Efstathiou, G., Ellis, R. S., & Peterson, B. A. 1988, M.N.R.A.S., 232, 431.
- Ellis, R. S., Colless, M., Broadhurst, T., Heyl, J., & Glazebrook, K. 1996, M.N.R.A.S., 280, 235.
- Ferguson, H. C., & McGaugh S. S. 1995, Ap. J., 440, 470.
- Freeman, K. 1970, Ap. J., 160, 811.
- Glazebrook, K., Peakcock, J. A., Colins, C. A., Miller, L. 1994, M.N.R.A.S., 266, 65.
- Gardner, J. P., Sharples, R. M., Carrasco, B. E., & Frenk, C. S. 1996, M.N.R.A.S., 282, L1.
- Humason, M. L., Hayall, N. U., & Sandage, A. R. 1956, A. J., 61, 97.
- Jorgensen, I., Franx, M., & Kjaergaard, P. 1995, M.N.R.A.S., 273, 1097.
- Knezek, P. 1993, Ph.D. Thesis, University of Massachusetts.
- Kron, R. G. 1980, Ap. J. Suppl., 43, 305.
- Lilly, S. J., Cowie, L. L., & Gardner J. P. 1991, Ap. J., **369**, 79.
- Lilly, S. J., Le Fèvre, O., Crampton, D., Hammer, F., & Tresse, L. 1995a Ap. J., 455, 50.
- Lilly, S. J., Tresse, L., Hammer, F., Crampton, D., Le Fèvre, O. 1995b Ap. J., 455, 108.
- Lin, H., Kirshner, R. P., Shectman, S. A., Landy, S. D., Oemler, A., Tucker, D. L., & Schechter P. L. 1996, Ap. J., 464, 60.
- Lin, H., Yee, H. K. C., Carlberg, R. G., & Ellingson, E. 1997, Ap. J., 475, 494.
- McGaugh, S. S. 1994, Nature, 367, 538.
- McGaugh, S. S., & Bothun, G. D. 1994, A. J., 107, 530.
- McGaugh, S. S., Bothun, G., & Schombert, J. 1995, A. J., 110, 573.
- Moffat, A. F. J. 1969, Astr. Ap., 3, 455.
- Petrosian, V. 1976, Ap. J. (Letters), , 209, 1.
- Phillipps, S., Davies, J. I., & Disney, M. J. 1990, M.N.R.A.S., 242, 235.
- Phillipps, S., & Driver, S. 1995, M.N.R.A.S., 274, 832.
- Ratnatunga, K. U., Griffiths, R. W., & Casertano, S. 1994, in The Restoration of HST Images and Spectra-II, ed. R. J. Hanisch & R. L. White (Baltimore: STScI), 222.
- Reeves, G. 1956, A. J., 61, 69.
- Romanishin, W., Strom, K. M., & Strom, S. E. 1983, Ap. J. Suppl., 53, 105.

- Sandage, A., 1961, *Ap. J.*, 133, 355.
- Sandage, A., Tammann, G. A., & Yahil, A. 1979, *Ap. J.*, 232, 352.
- Schechter, P. 1976 *Ap. J.*, 203, 297.
- Schade, D., Lilly, S. J., Le Fevre, O., Hammer, F., & Crampton, D. 1996, *Ap. J.*, 464, 79.
- Schombert, J. M., Bothun, G. D., Schneider, S. E., & McGaugh, S. S. 1992, *A. J.*, 103, 1107
- Shectman, S., Landy, D., Oemler, A., Tucker, D., Lin, H., Kirshner, R., & Schechter, P. 1996, *Ap. J.*, 470, 172
- Small, T. A., & Sargent, W. L. W. 1997, *Ap. J. Suppl.*, , 111.
- Valdes, F. 1982, *S.P.I.E.*, 331, 465.
- de Vaucouleurs, G., de Vaucouleurs, A., Corwin, H. G., Buta, R. J., Paurel, G., & Fouqué, P. 1991, *Third Reference Catalogue of Bright Galaxies* (Springer, New York).
- Wirth, D. 1996, Ph. D. Thesis, University of California at Santa Cruz.
- Yee, H. K. C., Ellingson, E., & Carlberg, R. C. 1996, *Ap. J. Suppl.*, 102, 269.
- Yoshii, Y. 1993, *Ap. J.*, 403, 552.

Table 1. Photometric Parameters for Some Recent Faint Field Surveys

Survey	Band	Seeing ($''$)	Magnitude Limits	Limiting Surface Brightness	
				Photometry	Detection
CFRS ^a	I_{AB}	$0.6'' - 1''$	$17.5 < I_{AB} < 22.5$	$28.0 I_{AB}/\square''$	$25.5 I_{AB}/\square''$
LCRS ^b	Gunn- r	$\sim 1.3''$	$15 \leq r_{iso} \leq 17.7$	$\sim 23 r/\square''$	$\sim 22 r/\square''$
CNOC ^c	Gunn- r, B_{AB}	?	$r < 20.5, 21.5, 22.0$	^j	?
AutoFib ^{d,e}	b_J	?	$19.5 < b_J < 22$	$26.5 b_J/\square''$	$\sim 25 b_J/\square''$
Norris ^f	Gunn- r, B_{AB}	$\sim 2.0''$	$r_{core} \leq 21.7, r_{tot} < 20$	^k	$24.1 r/\square''$
Gardner ^g	K^i	?	$K \leq 15$	^l	$22.5 I, 18.5 K/\square''$
Glazebrook ^h	K	$1.9'' - 3.5''$	$K \lesssim 17$	^m	$\sim 19 K/\square''$

^aLilly et al. 1995a

^bShectman et al. 1996

^cYee et al. 1996, Lin et al. 1997

^dEllis et al. 1996

^eParameters refer only to AutoFib-faint sample; luminosity function includes data from other surveys with different selection criteria

^fSmall et al. 1997

^gGardner et al. 1996

^hGlazebrook et al. 1994

ⁱ K photometry performed only for galaxies detected in I

^jVariable aperture magnitudes used

^kFOCAS total magnitudes used

^l $10''$ apertures used

^m $4'' - 8''$ apertures used, depending on seeing.

9. Figure Captions

Fig. 1.— [a] The fraction of the light detected above a limiting isophote, represented as the error in the derived absolute magnitude (i.e. $\Delta M(z) = -2.5 \log f(z)$), is plotted as a function of redshift, for different seeing (from top to bottom: FWHM=0.1", 1.0", 2.0", for a Moffat profile with $\beta = 5$), different galaxy surface brightnesses relative to the limiting isophote (left to right: $\Delta\mu = \mu_{lim} - \mu_0 = 7, 5, 3, 1$), and different galaxy sizes ($\alpha = 0.25$ kpc, 1 kpc, 3 kpc: dashed, dotted, and solid lines, respectively), for circularly symmetric galaxies with exponential surface brightness distributions. $f(z)$ includes the effect of cosmological dimming on reducing the fraction of light seen at high redshift, but does not include the k -correction, which can modify the effective central surface brightness at high redshift. We have assumed $H_0 = 50$ km/s/Mpc and $\Omega_0 = 1$. For larger values of the Hubble constant, the upturn in $\Delta M(z)$ will occur at larger redshifts; however, the characteristic size of the galaxies in Figure 2 will become smaller. [b] Same as [a], but for a de Vaucouleurs profile. See Figure 5 for a treatment of aperture magnitudes and Petrosian magnitudes.

Fig. 2.— The values of μ_0 and α for a variety of galaxy samples. The solid circles and open squares are spiral bulges and spiral disks, respectively, drawn from de Jong (1996a), and the asterisks are ellipticals in A157 and A3574 from Jorgensen et al. (1995). The solid triangles are low surface brightness galaxies (LSBs) from the UGC catalog from Knezek (1993). The crosses are spiral disks from an assortment of other sources (Romanishin et al. 1973, Boroson 1981, van der Kruit 1987, Sprayberry et al. 1995, de Blok et al. 1995, McGaugh & Bothun 1994) and are primarily selected from the NGC, UGC, or POSS-II catalog of LSBs (Schombert et al. 1992), all of which are either explicitly or implicitly angular diameter limited field surveys. The stars are the local group dwarf spheroidals compiled by Caldwell et al. 1992. The dashed line is the locus of $M_B = -20$. For the de Vaucouleurs profile galaxies (asterisks and filled circles), the conversion from effective radius r_e and effective surface brightness μ_e to μ_0 and α is as given in the text. All data has been converted to the Johnson B magnitude system. The data are chosen to represent the existing range of galaxy morphologies and luminosities, and not to argue for a particular relation between α and μ_0 for a given profile type.

Fig. 3.— The luminosity functions (left column) and V/V_{max} distributions (right column) for samples of galaxies with different central surface brightnesses [(a) $\mu_0 = 20$ mag/arcsec², (b) $\mu_0 = 22$ mag/arcsec², & (c) $\mu_0 = 24$ mag/arcsec² for exponential profile galaxies, and (d) $\mu_0 = 20$ mag/arcsec², (e) $\mu_0 = 22$ mag/arcsec², & (f) $\mu_0 = 24$ mag/arcsec² are for de Vaucouleurs profile galaxies], calculated using standard methods (heavy lines; eqn. 1), and calculated using the proper corrections for lost light (light lines; eqn. 2). The upper row is the luminosity function and V/V_{max} distribution derived from the entire sample. The middle row is for the galaxies which fall below the mean redshift of the sample, and the lower row is for the galaxies falling above the mean redshift; the mean redshift changes with surface brightness. For the cases where the luminosity function appears to evolve with redshift, Schechter luminosity function fits are plotted superimposed to facilitate comparison; the dotted line in the lower left panel is the luminosity function fit to the low redshift data. All samples have 5,000 galaxies, and assume a limiting isophotal magnitude of $m_{lim} = 25$ mag/arcsec², measured within an outer isophote of $\mu_{lim} = 22$ mag/arcsec², and 1" seeing, with a $\beta = 5$ Moffat profile distribution. They do not include the effects of random galaxy inclinations. Note that the luminosity function has a higher normalization for the lower surface brightness galaxies, due to the systematically lower accessible volume, and thus the smaller mean sample redshift (Figure 1; also Phillipps et al. 1990 and references therein).

Fig. 4.— The first moment radius r_1 measured above some limiting surface brightness μ_{lim} (upper panel) and the resulting error in the absolute Kron magnitude measured within $2r_1$ (i.e. $\Delta M = -2.5 \lg f(2r_1)$), lower

panel), as a function of $\Delta\mu = \mu_{lim} - \mu_0$, for different angular scale lengths $\alpha = 0.25''$, $1''$, & $2''$ in the presence of a Moffat PSF with $FWHM = 1''$, for [a] exponential disks and [b] de Vaucouleurs' profile ellipticals. Lower surface brightness galaxies (small $\Delta\mu$) have systematically underestimated Kron magnitudes, because the value of r_1 is underestimated when only a fraction of the galaxy's profile is used to calculate r_1 . Elliptical galaxies, which have a larger fraction of light at large radii, are subject to larger errors in the measured luminosity than exponential disks. The curves are purely theoretical, and do not take noise and other forms of measurement error into account. For reference, when measured within $r \rightarrow \infty$, $r_1(\infty)/\alpha = 2$ for a pure exponential profile, and $r_1(\infty)/\alpha = 3.8424$ for a pure de Vaucouleurs' profile. The biases are identical for the same for galaxies with the same ratio of the $FWHM$ to the scale length α .

Fig. 5.— The error in the measured absolute magnitude as a function of redshift, for aperture and Petrosian magnitudes (top and bottom, respectively), for both exponential (left) and de Vaucouleurs (right) profile galaxies, in the presence of a $1''$ FWHM Moffat profile PSF with $\beta = 5$ (comparable to the middle row of Figure 1). As in Figure 1, the different lines represent galaxies of different physical sizes ($\alpha = 0.25$ kpc, 1 kpc, 3 kpc: dashed, dotted, and solid lines, respectively). Because both aperture and Petrosian magnitudes scale linearly with surface brightness, the given plots of ΔM are independent of galaxy surface brightness. Note the factor of 5 difference in scale between the aperture magnitude plots and the Petrosian magnitude plots.

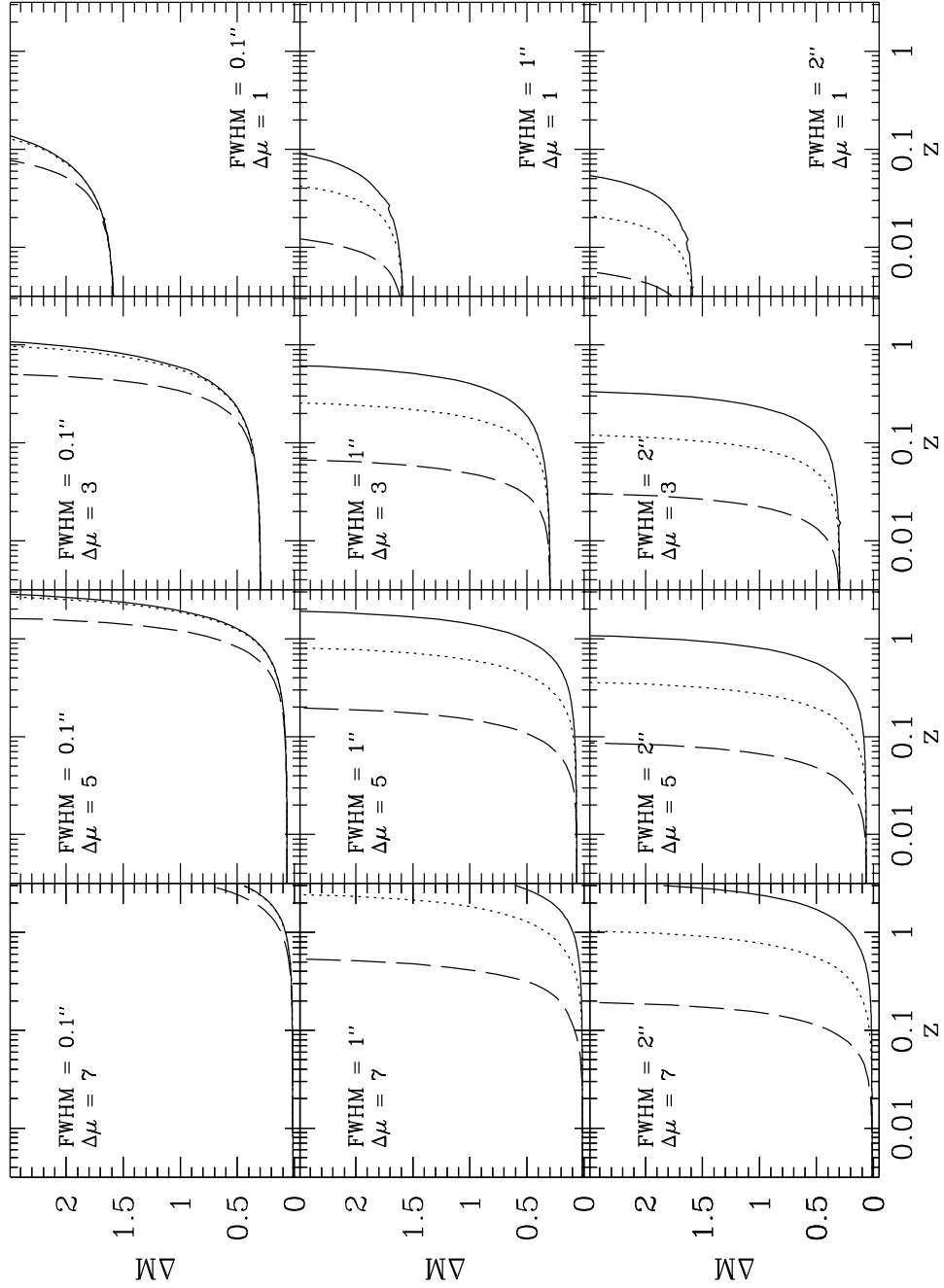


FIGURE 1[A]

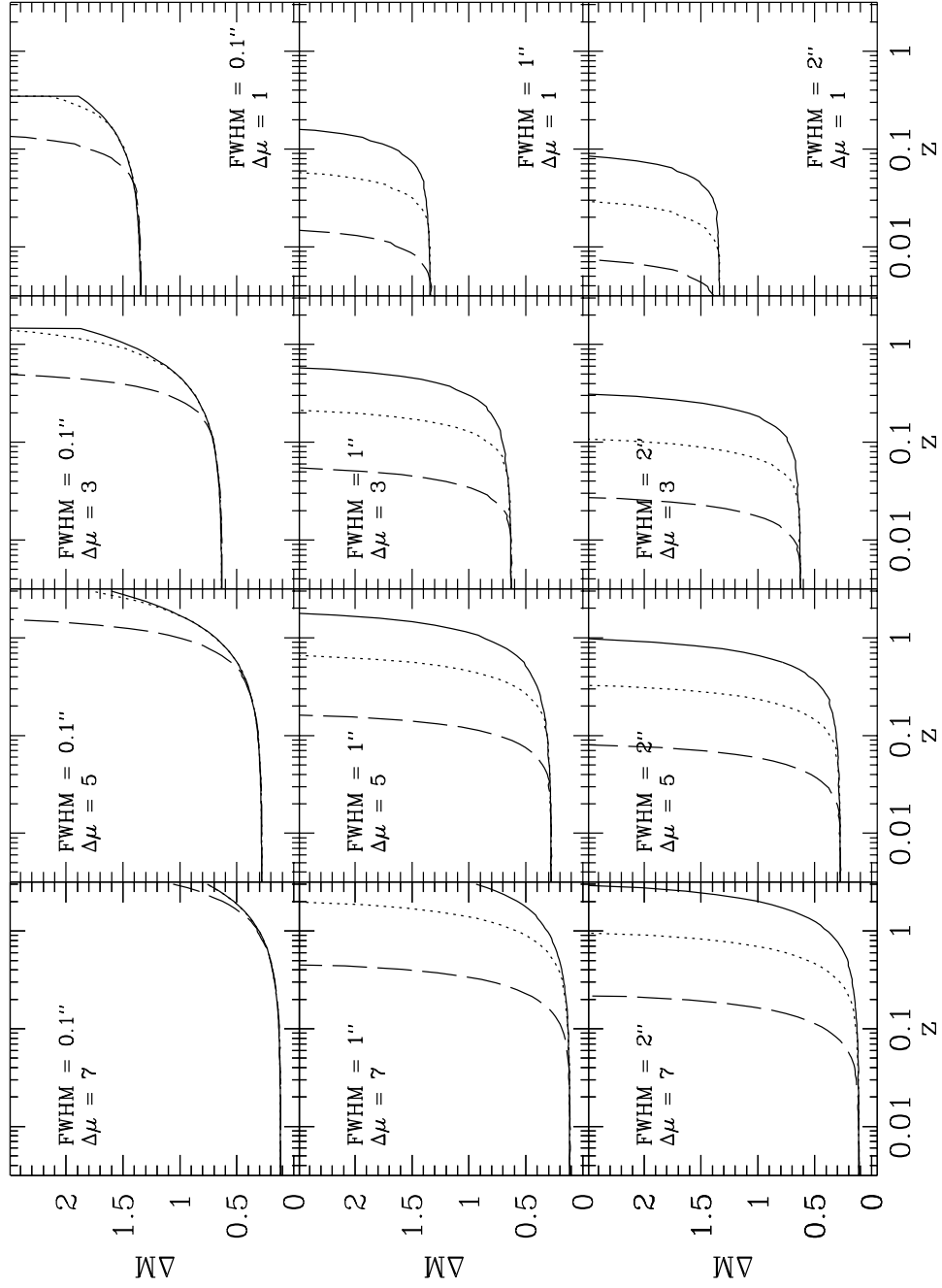


FIGURE 1[B]

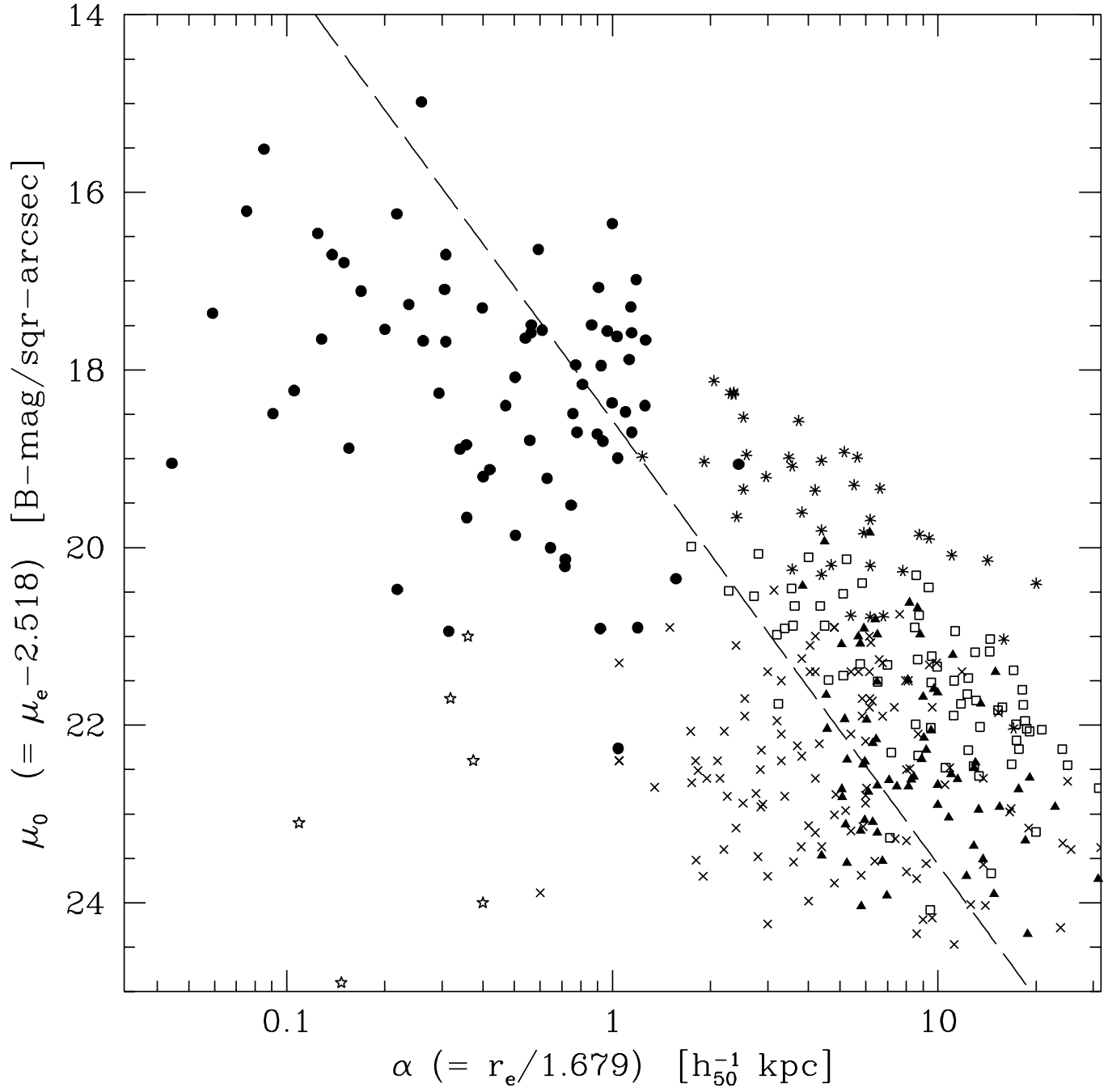


FIGURE 2

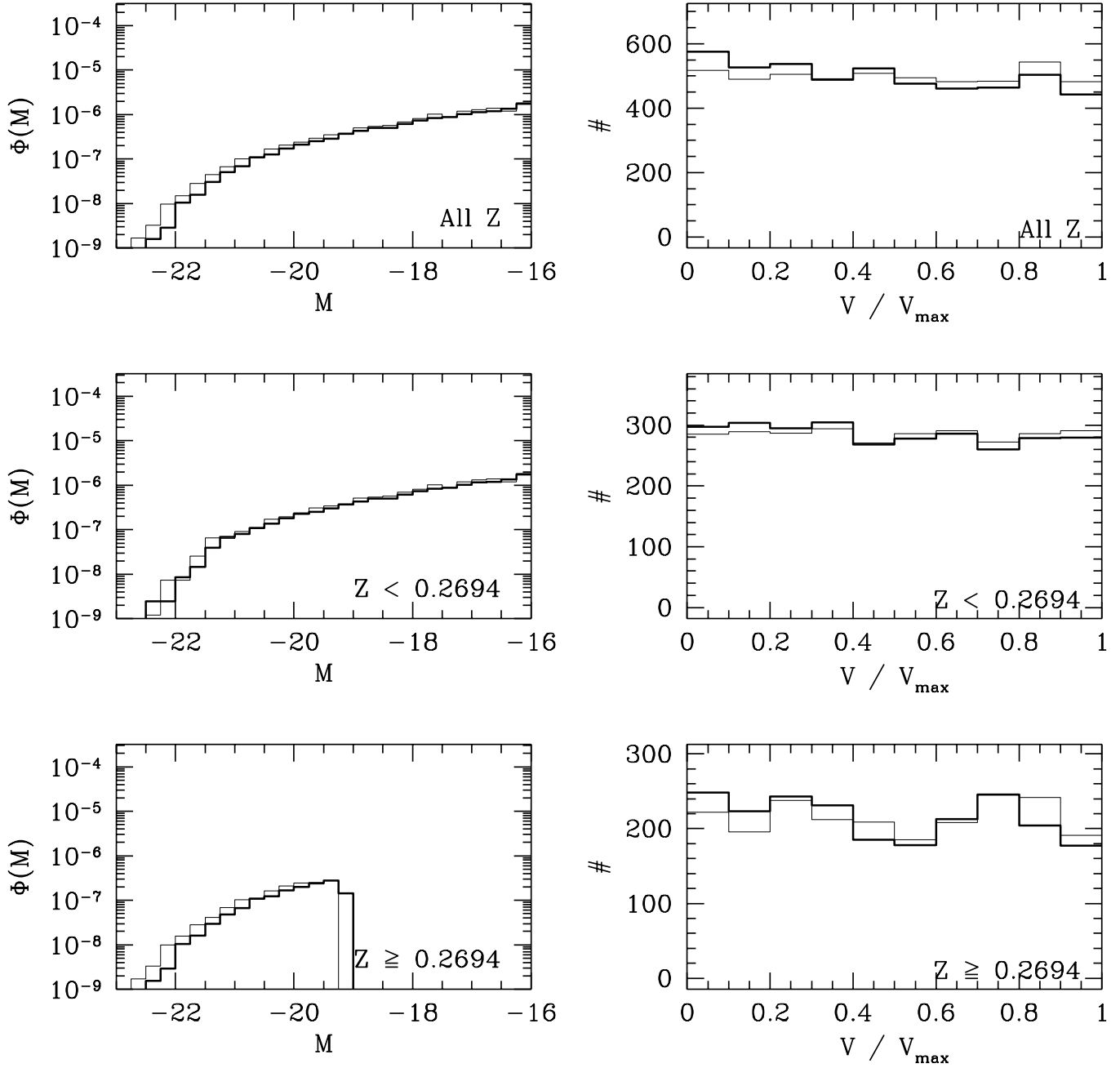


FIGURE 3[A]

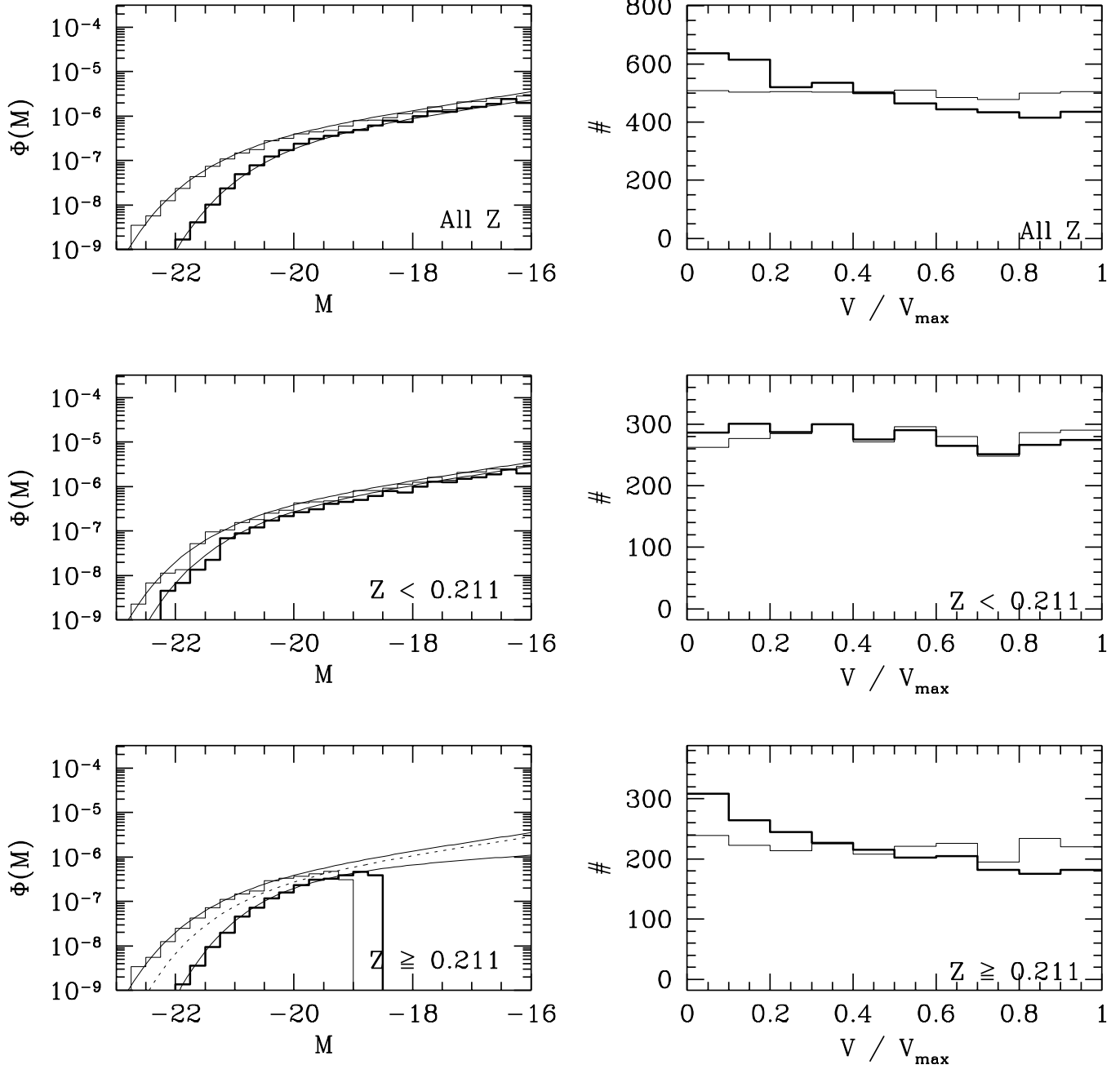


FIGURE 3[B]

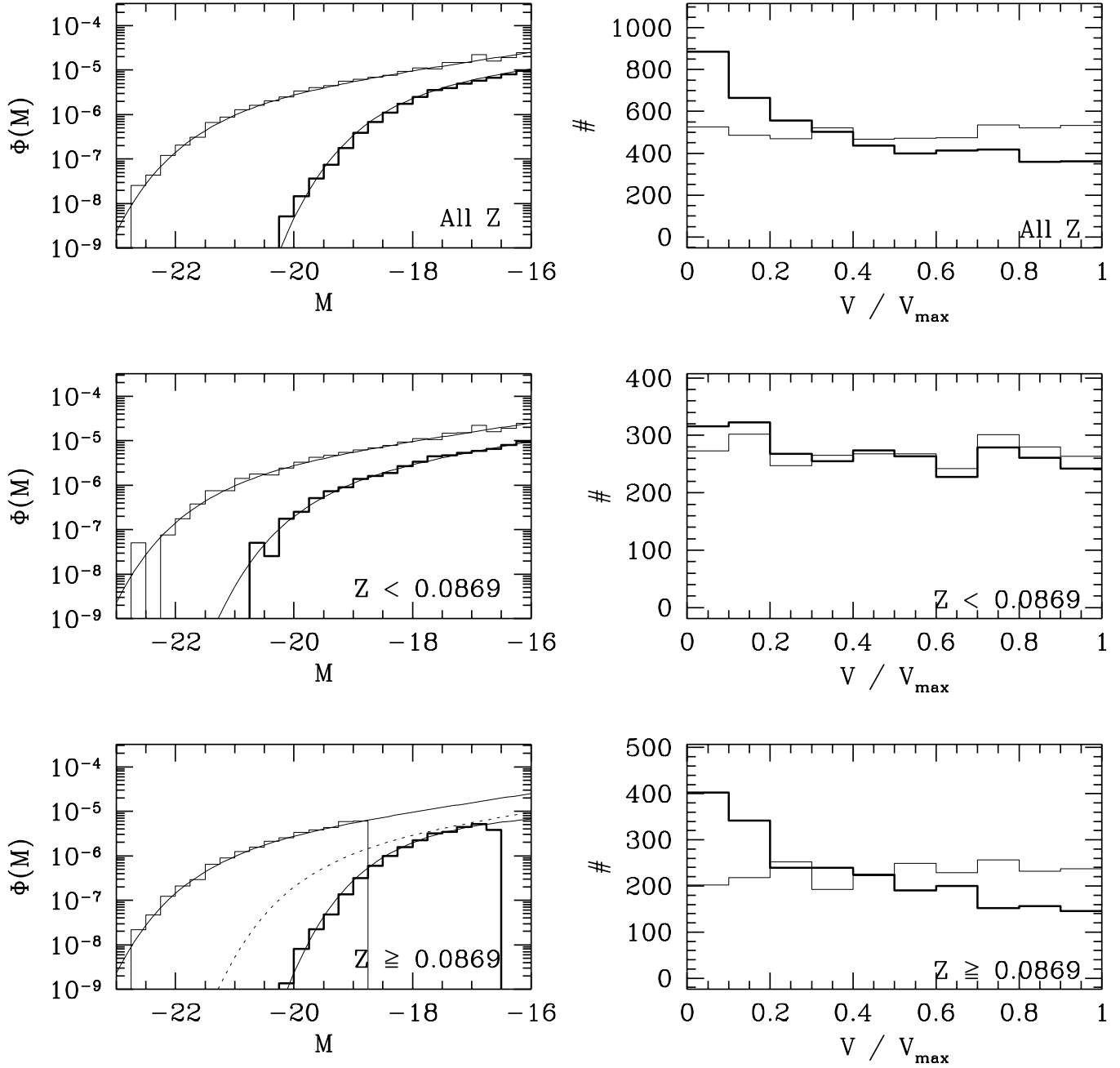


FIGURE 3[c]

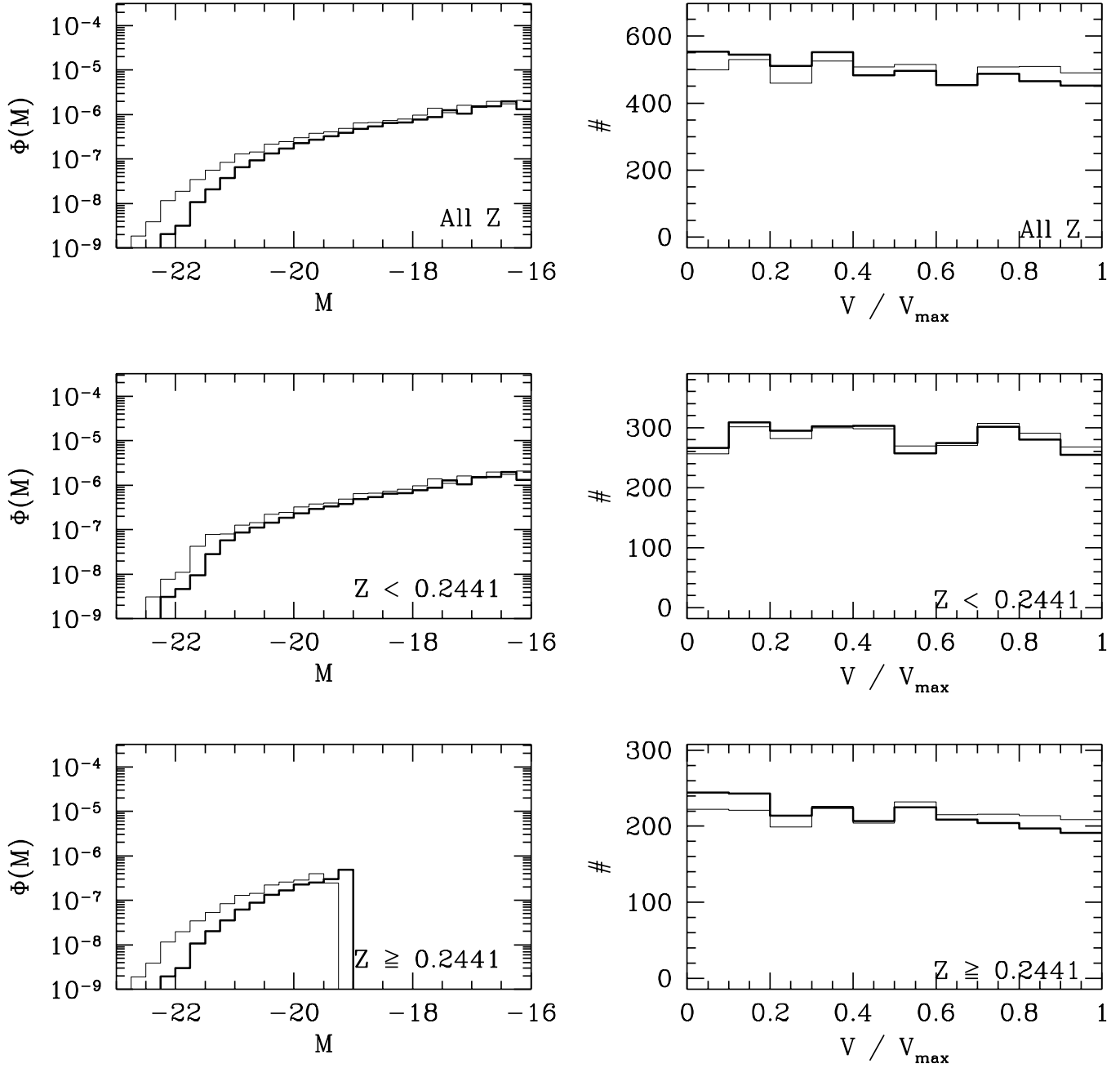


FIGURE 3[D]

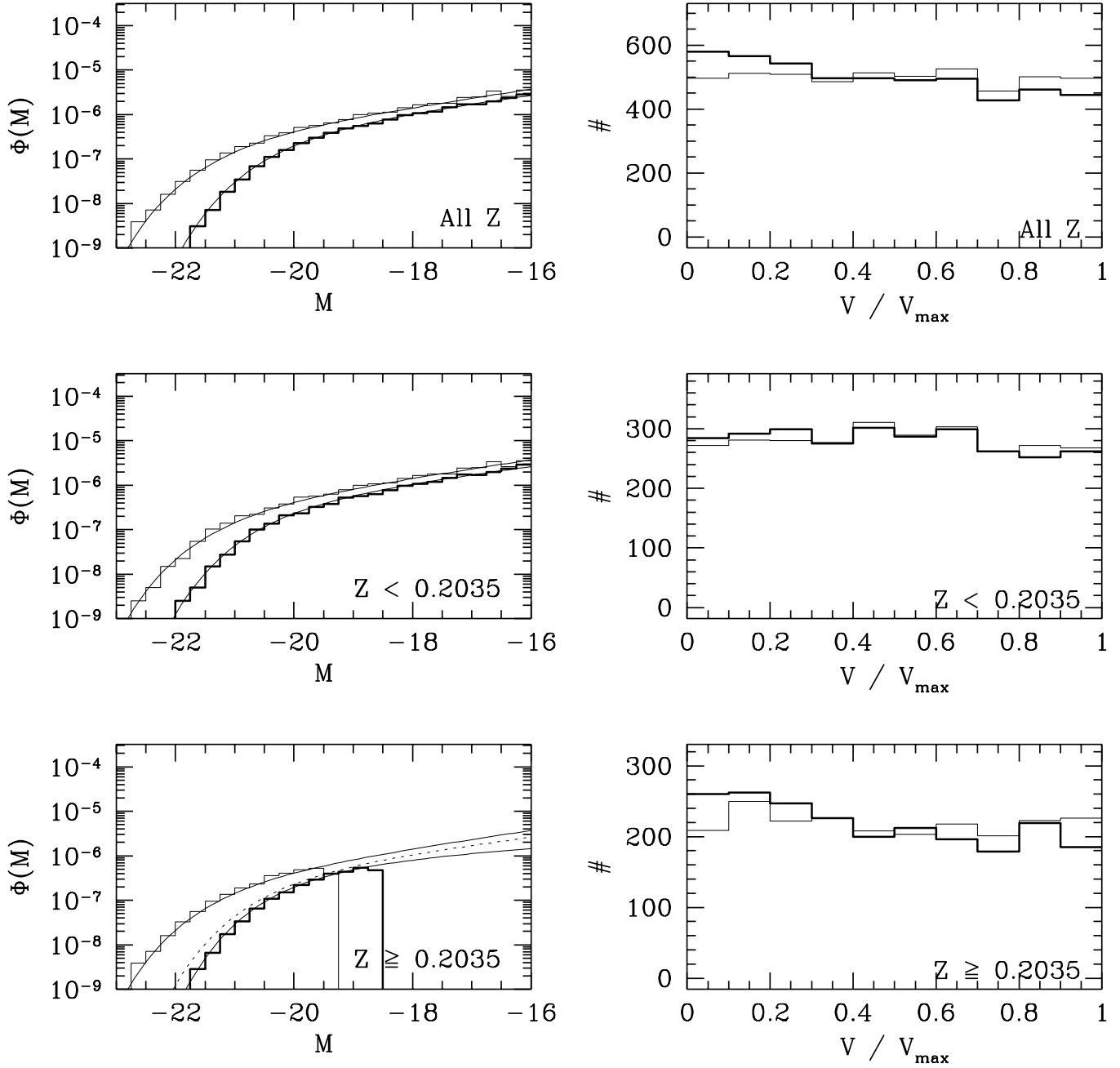


FIGURE 3[E]

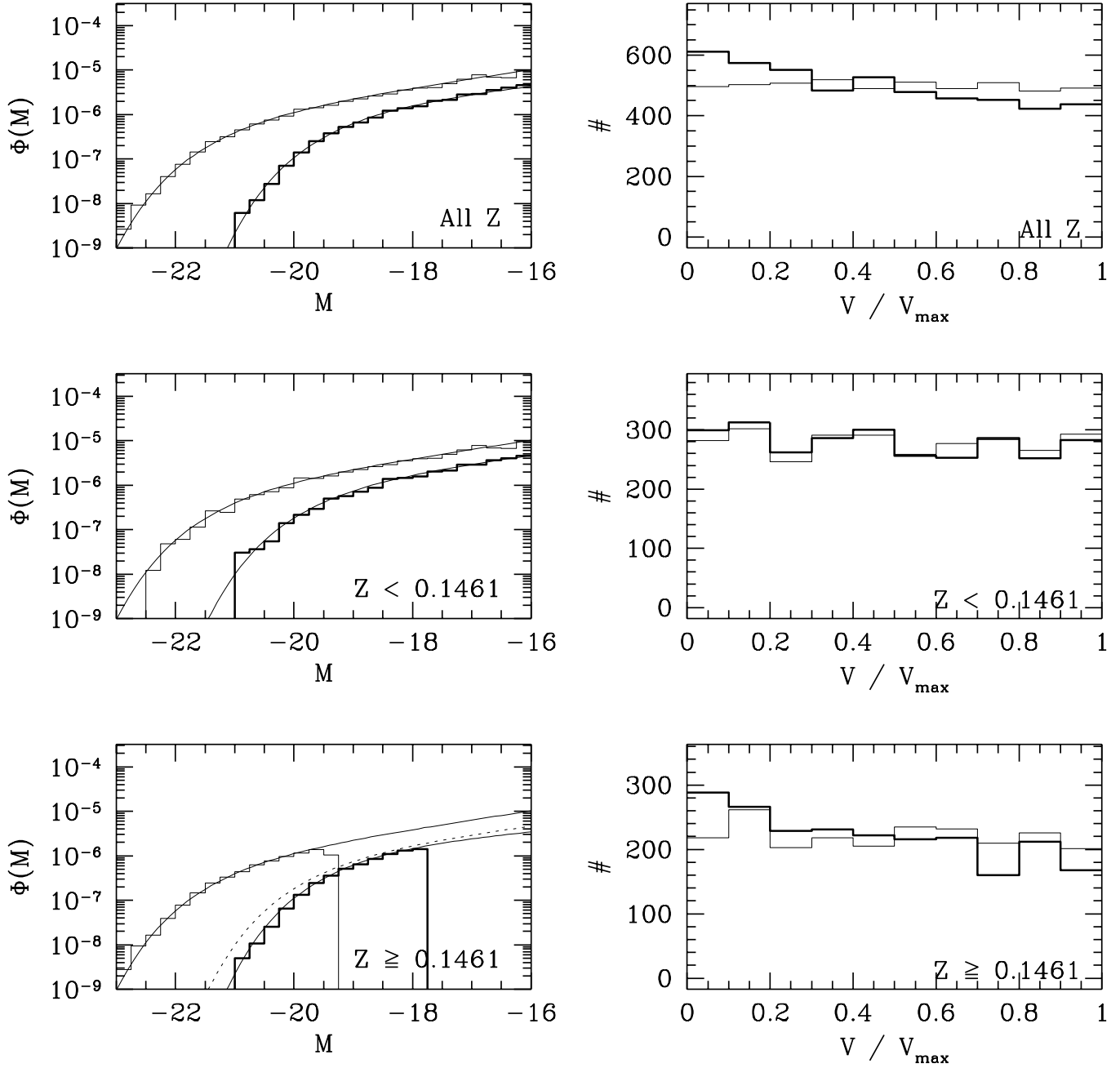


FIGURE 3[F]

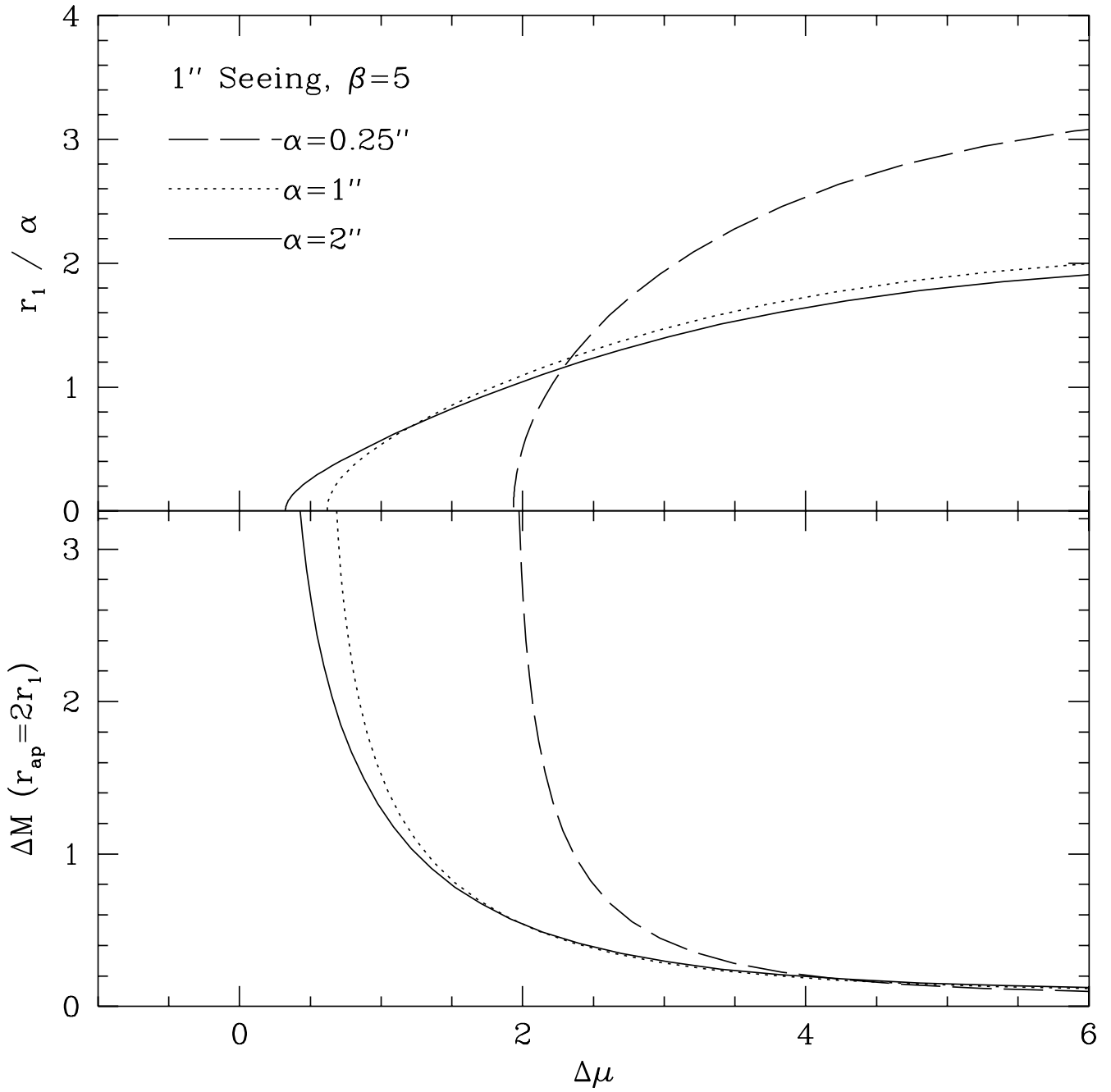


FIGURE 4[A]

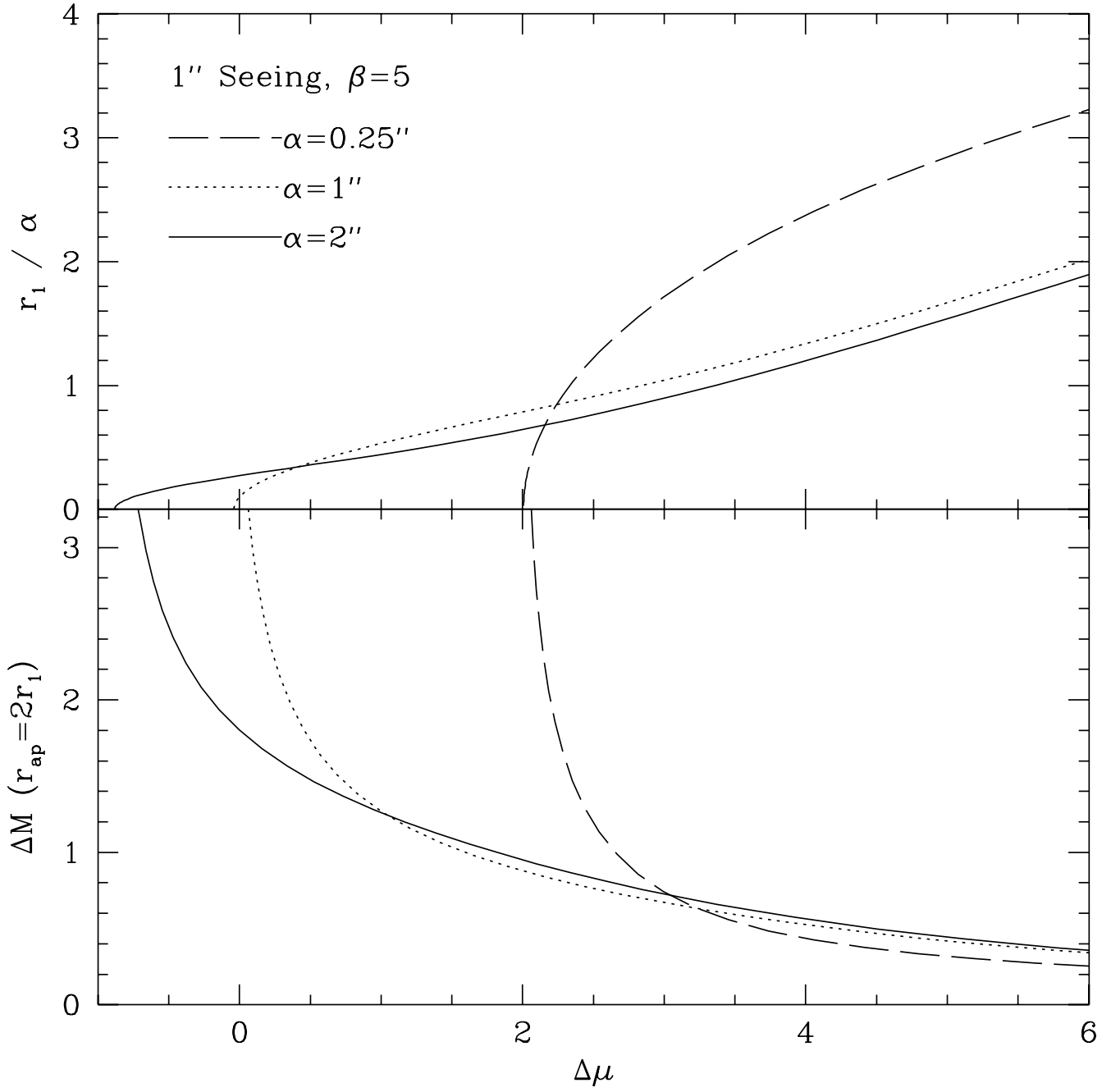


FIGURE 4[B]

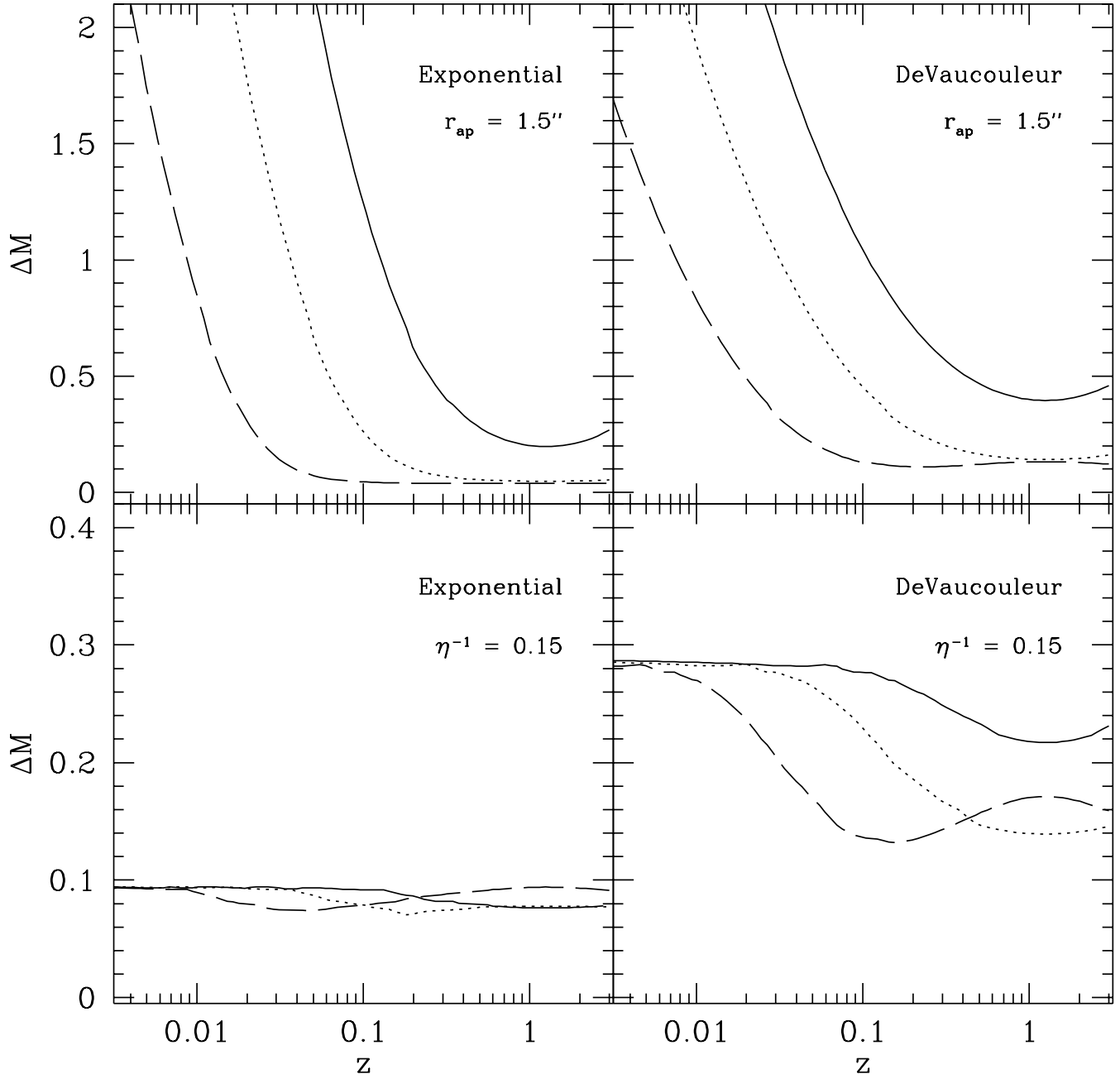


FIGURE 5